Photodissociation dynamics of nitrobenzene and o -nitrotoluene

Ming-Fu Lin, Yuan T. Lee, Chi-Kung Ni, Shucheng Xu, and M. C. Lin

Citation: The Journal of Chemical Physics **126**, 064310 (2007); doi: 10.1063/1.2435351
View online: http://dx.doi.org/10.1063/1.2435351
View Table of Contents: http://scitation.aip.org/content/aip/journal/jcp/126/6?ver=pdfcov
Published by the AIP Publishing

Photodissociation dynamics of nitrobenzene and *o*-nitrotoluene

Ming-Fu Lin, Yuan T. Lee,[a] and Chi-Kung Ni[b]
Institute of Atomic and Molecular Sciences, Academia Sinica, P.O. Box 23-166, Taipei, Taiwan

Shucheng Xu
Department of Chemistry, Emory University, Atlanta, Georgia 30322

M. C. Lin
Department of Chemistry, Emory University, Atlanta, Georgia 30322
and Center for Interdisciplinary Molecular Science, National Chiao Tung University, Hsinchu, Taiwan

(Received 8 September 2006; accepted 28 December 2006; published online 12 February 2007)

Photodissociation of nitrobenzene at 193, 248, and 266 nm and *o*-nitrotoluene at 193 and 248 nm was investigated separately using multimass ion imaging techniques. Fragments corresponding to NO and NO_2 elimination from both nitrobenzene and *o*-nitrotoluene were observed. The translational energy distributions for the NO elimination channel show bimodal distributions, indicating two dissociation mechanisms involved in the dissociation process. The branching ratios between NO and NO_2 elimination channels were determined to be $NO/NO_2 = 0.32 \pm 0.12$ (193 nm), 0.26 ± 0.12 (248 nm), and 0.4 ± 0.12(266 nm) for nitrobenzene and 0.42 ± 0.12(193 nm) and 0.3 ± 0.12 (248 nm) for *o*-nitrotoluene. Additional dissociation channels, O atom elimination from nitrobenzene, and OH elimination from *o*-nitrotoluene, were observed. New dissociation mechanisms were proposed, and the results are compared with potential energy surfaces obtained from *ab initio* calculations. Observed absorption bands of photodissociation are assigned by the assistance of the *ab initio* calculations for the relative energies of the triplet excited states and the vertical excitation energies of the singlet and triplet excited states of nitrobenzene and *o*-nitrotoluene. Finally, the dissociation rates and lifetimes of photodissociation of nitrobenzene and *o*-nitrotoluene were predicted and compared to experimental results. © *2007 American Institute of Physics*. [DOI: 10.1063/1.2435351]

I. INTRODUCTION

Nitrobenzene and nitrotoluene are prototypical molecules employed in studies of the combustion and decomposition of energetic materials. Early studies of nitrobenzene using discharge lamp photolysis and flash lamp photolysis found that photodissociation of nitrobenzene generates several different products, including nitrogen dioxide, nitrosobenzene, and cyclopentadiene.[1] Resonance enhanced multiphoton ionization study of nitrobenzene detected NO and a number of C_nH_m ($n=1-6$, $m=0-5$) fragments.[2] In a recent study, Galloway *et al.* employed vacuum ultraviolet (VUV) photoionization mass spectrometry to detect dissociation products in the photolysis of nitrobenzene at wavelengths between 220 and 280 nm.[3] The observed products can be attributed to the following three major channels:

$$C_6H_5NO_2 + h\nu \rightarrow C_6H_5 + NO_2, \quad (1)$$

$$C_6H_5NO_2 + h\nu \rightarrow C_6H_5NO + O, \quad (2)$$

$$C_6H_5NO_2 + h\nu \rightarrow C_6H_5O + NO(\text{or } C_6H_5 + CO + NO). \quad (3)$$

The dissociation mechanism was proposed to start from the internal conversion to the ground electronic state, followed by the isomerization to phenyl nitrite C_6H_5ONO, and subsequently breaking the C–ONO bond to release NO_2, or the O–NO bond to produce NO, or the ON–O bond to form O. Although no phenoxy radical was observed in the experiment, it was assumed that the phenoxy radical generated in reaction (3) further decomposed into C_5H_5+CO due to the large internal energy in C_6H_5O and low decomposition barrier. Rotational and vibrational energy distributions of the nitric oxide product after photodissociation of nitrobenzene at several wavelengths have been measured.[4] It was found that most of the NO was produced in $v=0$. The rotational state distributions of the nascent NO photofragment can be characterized by a Boltzmann temperature in the range of 2400–3700 K, depending on the photolysis wavelength. A statistical model with some adjustments was suggested for the explanation of NO rotational state distributions.

Dissociation of the nitrotoluene has also been studied. A femtosecond laser multiphoton ionization mass spectroscopic experiment at 375 nm showed that $C_7H_7^+$ and $C_7H_7O^+$, corresponding to NO_2 and NO loss channels, were observed for all three nitrotoluene isomers.[5] Ions of C_7H_7NO, corresponding to the loss of O fragments, were observed from *p*-nitrotoluene. In addition, ion of $m/e=120$, corresponding to OH loss, is a significant product from *o*-nitrotoluene. Dissociation occurs after multiphoton ionization was proposed

[a] Also at Department of Chemistry, National Taiwan University, Taipei, Taiwan.
[b] Also at Department of Chemistry, National Tsing Hua University, Hsinchu, Taiwan. Electronic mail: ckni@po.iams.sinica.edu.tw

to be the mechanism in the experiment. Bicyclic cation intermediates and, possibly, rearrangement to the nitrite form prior to fragmentation have been suggested to explain the OH loss channel of nitrotoluene cation.[6] On the other hand, NO product state distributions from the dissociation of neutral *o*-nitrotoluene have also been observed.[7] In these studies, the NO product internal energy distributions were unlike those from dissociation of nitrobenzene. Whether NO is generated from the isomerization pathway analogous to that of nitrobenzene is unclear.

The theoretical calculations for the geometries and energies of nitrobenzene in the ground electronic state and in singlet and triplet excited states have been performed by the complete active space self-consistent field (CASSCF) method.[8] Recently, theoretical studies on the kinetics and mechanisms for the thermal unimolecular decomposition of nitrobenzene and *o*-nitrotoluene have been carried out, respectively, by Xu and Lin[9] and by Chen *et al.*[10]

In this work, the photodissociation of nitrobenzene and *o*-nitrotoluene was investigated separately using a multimass ion imaging technique.[11] Photofragment translational energy distributions and dissociation rates were measured. A new dissociation mechanism was proposed by the assistance of the *ab initio* calculations for the potential energy surfaces and the excitation energies of the excited states of nitrobenzene and *o*-nitrotoluene.

II. EXPERIMENT

The experimental technique has been described in detail in our previous reports on other aromatic molecules.[11] Only a brief description is given here. Nitrobenzene (or *o*-nitrotoluene) vapor was formed by flowing ultrapure He at pressures of 800 (or 500) Torr through a reservoir filled with a sample at 350 (or 330) K. The sample/He mixture was then expanded through a 500 μm pulsed nozzle to form the molecular beam. Molecules in the molecular beam were photodissociated by an UV laser pulse. Due to the recoil velocity and center-of-mass velocity, the fragments were distributed on an expanding sphere on their flight to the ionization region and then ionized by a VUV laser pulse. The distance and time delay between the VUV laser pulse and the UV photolysis laser pulse were set long enough such that the radius of the fragment sphere is at least larger than 1 cm. The delay time of the VUV laser pulse was also set such that the VUV laser beam passed through the center of mass of the dissociation products. Since the diameter of the VUV laser beam (<1 mm) is much smaller than the radius of the fragment sphere, it generated a line segment of photofragment ions by photoionization. The length of the segment was proportional to the fragment recoil velocity in the center-of-mass frame multiplied by the delay time between the photolysis and the ionization laser pulses. To separate the different masses within the ion segment, a pulsed electric field was used to extract the ions into a mass spectrometer after ionization. While the mass analysis was being executed in the mass spectrometer, the length of each fragment ion segment continued to expand in the original direction according to its recoil velocity. At the exit port of the mass spectrometer, a two-dimensional ion detector was used to detect the ion positions and intensity distribution. In this two-dimensional detector, one direction was the recoil velocity axis and the other was the mass axis. The translational energy distributions of many different fragments therefore can be measured simultaneously from the image.

If the dissociation rate was small, then some molecules did not dissociate immediately after the absorption of photolysis photons. Those molecules with large internal energy stayed within the molecular beam. They flew with almost the same velocity to the ionization region and then were ionized by the VUV laser, resulting in dissociative ionization. The ion image from dissociative ionization is very different from the image due to the dissociation products of neutral molecules. Since the dissociation and ionization occurred at the same position, the image from dissociative ionization is a two-dimensional projection of the photofragment ion's three-dimensional recoil velocity distribution. It is a disklike image and is different from the line shape image resulting from dissociation products of neutral molecules. With the VUV laser fixed in position, only the intensity of the disklike image changed with the delay time between two laser pulses, but the size of the disklike image does not change with the delay time. Therefore, the ion image resulting from dissociative ionization can be distinguished easily from the image resulting from dissociation products of neutral molecules by the shape of the image as well as the change with the delay time. The dissociation rate was obtained from the measurements of product growth and the excited parent molecule intensity decay (disklike image intensity decay) with respect to the delay time between the pump and probe laser pulses using a time-of-flight mass spectrometer.

III. COMPUTATION

The geometries of the ground electronic (S_0) state and the triplet excited (T_1) state of nitrobenzene and *o*-nitrotoluene have been optimized at the B3LYP/6-311G(d,p) level. The relative energy of T_1 was calculated using a higher level calculation with the G2M(RCC, MP2) scheme[12] based on the optimized geometry at the B3LYP/6-311G(d,p) level. In addition, time-dependent density functional theory[13] (TD-DFT) calculation at the B3LYP/6-311G(d,p) level using the optimized geometries of the S_0 and T_1 states at the same level has been performed to predict the vertical excitation energies and oscillator strengths for the electronic excited states S_1–S_8 and T_2–T_8 of both molecules, respectively.

Ab initio calculations were carried out by GAUSSIAN 03 (Ref. 14) and MOLPRO 98 programs.[15] The dissociation rates and lifetimes for the photodissociation of nitrobenzene and *o*-nitrotoluene at 193 and 248 nm were predicted by the Rice-Ramsperger-Kassel-Marcus (RRKM) theory using the VARIFLEX code[16] or the CHEMRATE program.[17]

IV. RESULTS AND DATA ANALYSIS

A. Photodissociation channels of nitrobenzene

Ions of m/e=30(NO), 39(C_3H_3), 46(NO_2), 50(C_4H_2), 51(C_4H_3), 65(C_5H_5), and 77(C_6H_5) were observed from the

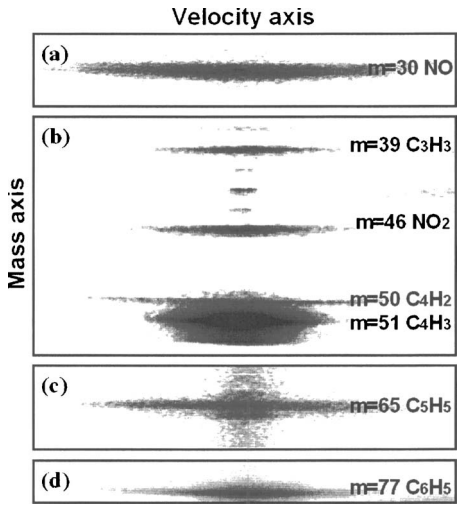

FIG. 1. Photofragment ion images from the photodissociation of nitrobenzene at 193 nm. The VUV wavelength is 118 nm.

photodissociation of nitrobenzene at 193 nm. Photolysis laser intensities in the region of 0.1–2 mJ/cm^2 were used to determine the photon number dependence of these fragments. The results show that except $m/e=39$ and 50, all photofragments stemmed from the dissociation of one-photon absorption. Only the fragments from one-photon dissociation will be discussed in this work. Figure 1 depicts the photofragment ion images obtained from the photodissociation of nitrobenzene at 193 nm using the 118.2 nm VUV laser beam. Fragments $m/e=30(NO)$, $46(NO_2)$, $65(C_5H_5)$, and $77(C_6H_5)$ have line shape images. They resulted from the dissociation of nitrobenzene.

The momentum distributions between C_6H_5 and NO_2 match very well, indicating the occurrence of reaction (1). The translational energy of this channel is shown in Fig. 2.

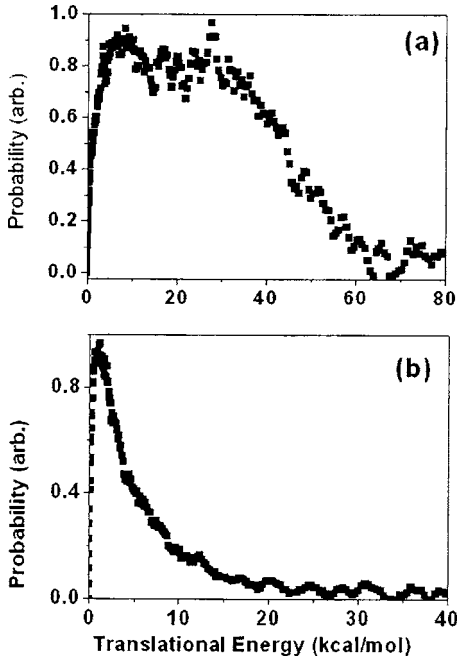

FIG. 2. Photofragment translational energy distribution of nitrobenzene at 193 nm. (a) $C_6H_5NO_2 \rightarrow C_6H_5O+NO$ and (b) $C_6H_5NO_2 \rightarrow C_6H_5+NO_2$.

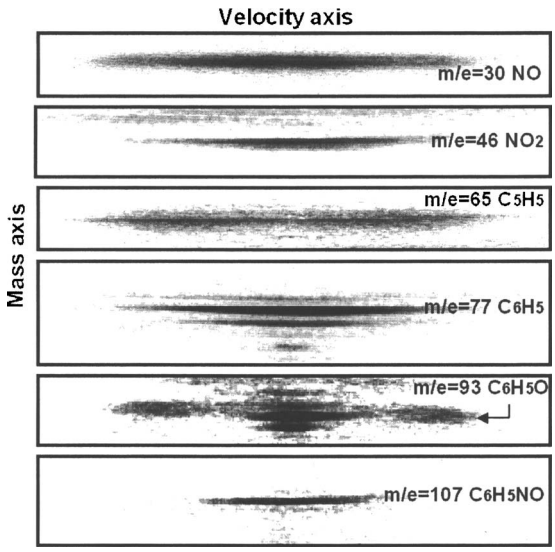

FIG. 3. Photofragment ion images from the photodissociation of nitrobenzene at 248 nm. The VUV wavelength is 118 nm.

The peak of the distribution is very close to zero, and it decreases rapidly as the translational energy increases. Although fragment NO was observed, no heavy fragment, C_6H_5O, corresponding to NO elimination was found. Only C_5H_5 was observed. Since most NO molecules (90%) are distributed in $v=0$ (Ref. 4) and the decomposition barrier for the reaction $C_6H_5O \rightarrow C_5H_5+CO$ is only 44 kcal/mol,[18] it is likely that C_6H_5O further decomposes into C_5H_5 and CO due to the large internal energy and low barrier height. The translational energy distribution measured from the NO fragment for the reaction $C_6H_5NO_2 \rightarrow C_6H_5O+NO$, as shown in Fig. 2, indicates a bimodal distribution.

Fragments $m/e=51(C_4H_3)$ has a disklike image. The size of the disk also changes slowly with the delay time. Instead of dissociative ionization from the undissociated parent molecules, it must be from the dissociative ionization of some heavy fragments. Indeed, the disklike image of $C_4H_3^+$ is from the fragment cracking of C_6H_5,

$$C_6H_5 \rightarrow C_4H_3^+ + C_2H_2. \quad (4)$$

The disklike image of $m/e=51$, resulting from reaction (4) can be further confirmed from the photodissociation of nitrosobenzene. In photodissociation of nitrosobenzene, the major channel is NO elimination. However, a disklike image at $m/e=51$ was also observed.

The similar dissociation channels were found in the photodissociation of nitrobenzene at 248 and 266 nm. The fragment ion images and the corresponding translational energy distributions are shown in Figs. 3–6. It is interesting to note that the fast component in the translational energy distribution of the NO elimination channel becomes small as the photolysis wavelength increases, and some of the heavy fragment of the NO elimination channel, C_6H_5O, does not completely decompose into C_5H_5+CO due to the small available energy. This fragment can be observed clearly, especially for the fast component, as illustrated in Fig. 3. In addition, a new fragment, C_6H_5NO, corresponding to O atom elimination

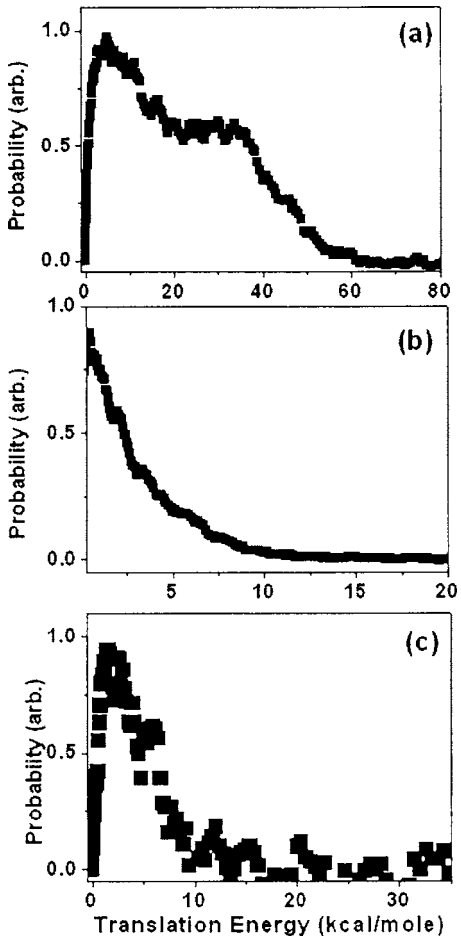

FIG. 4. Photofragment translational energy distribution of nitrobenzene at 248 nm. (a) $C_6H_5NO_2 \rightarrow C_6H_5O+NO$, (b) $C_6H_5NO_2 \rightarrow C_6H_5+NO_2$, and (c) $C_6H_5NO_2 \rightarrow C_6H_5NO+O$.

was observed. It was observed at both 248 and 266 nm. However, the fragment intensity at 266 nm was too small to be analyzed.

Dissociation rates were obtained from fitting the experimental data to $A\exp(-kt)+B(1-\exp(-kt))$, where $k=\Sigma_i k_i$. Here, k_i is the dissociation rate constant for channel i. The first term, $A\exp(-kt)$, represents the contribution from the decay of parent molecules (dissociative ionization) and the second term, $B(1-\exp(-kt))$, represents the growth of products generated from neutral molecule dissociation. The dissociation rates of nitrobenzene due to the 193 or 248 nm

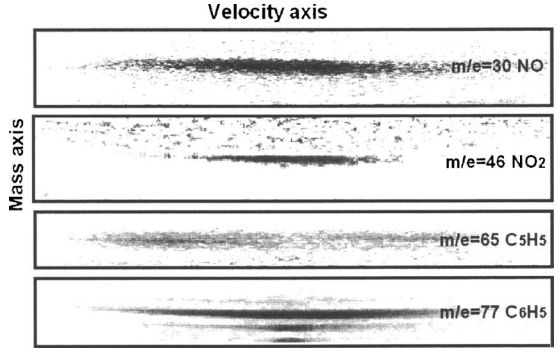

FIG. 5. Photofragment ion images from the photodissociation of nitrobenzene at 266 nm. The VUV wavelength is 118 nm.

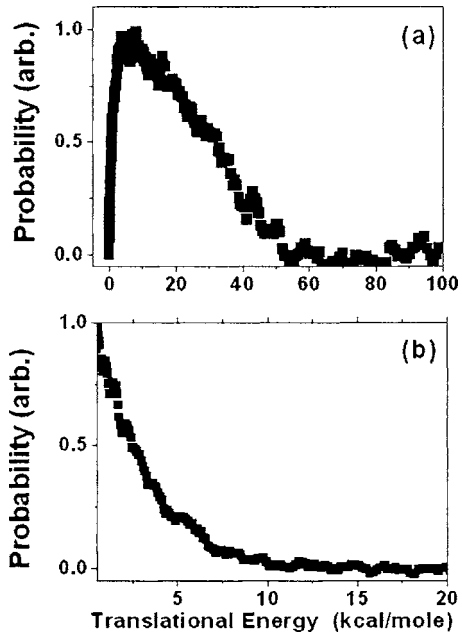

FIG. 6. Photofragment translational energy distribution of nitrobenzene at 266 nm. (a) $C_6H_5NO_2 \rightarrow C_6H_5O+NO$ and (b) $C_6H_5NO_2 \rightarrow C_6H_5+NO_2$.

photon excitation were found to be very close to our instrument time response. The actual dissociation rates at these wavelengths must be larger than 7×10^7 s^{-1}. On the other hand, the dissociation rate at 266 nm is slow enough to be measured, as shown in Fig. 7. It was found to be 1.7×10^7 s^{-1}.

B. Photodissociation channels of nitrotoluene

The largest image intensities we observed at 248 nm is the line shape images of $m/e=46(NO_2)$ and $91(C_6H_4CH_3)$,

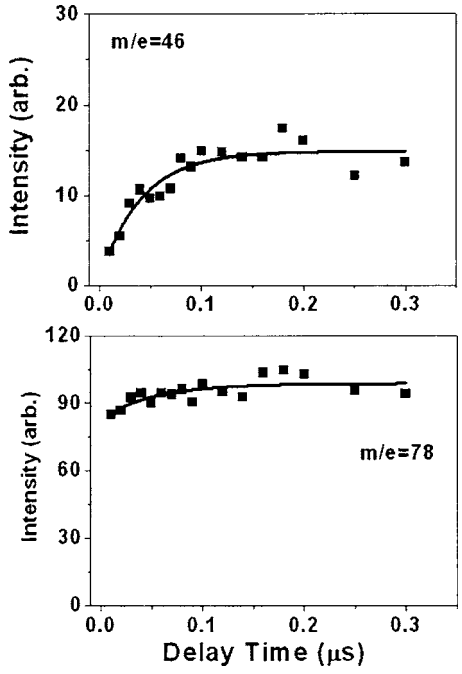

FIG. 7. Fragment ion intensity changes with respect to the delay time between pump and probe laser pulses. The photolysis wavelength is 266 nm; the VUV laser is 118.2 nm. Solid squares are the experimental data; solid lines are the fit to $A\exp(-kt)+B\times(1-\exp(-kt))$.

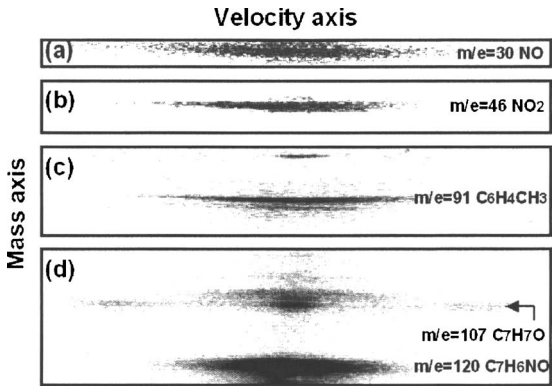

FIG. 8. Photofragment ion images from the photodissociation of *o*-nitrotoluene at 248 nm. The VUV wavelength is 118 nm.

as illustrated in Fig. 8. They correspond to the fragments of NO_2 and $C_6H_4CH_3$ from the NO_2 elimination channel. On the other hand, small intensities were observed from the line shape images of $m/e=30(NO)$ and $107(C_6H_4CH_3O)$. They represent the fragments of NO and $C_6H_4(CH_3)O$, resulting from the NO elimination channel. In addition, ions of $m/e=120(C_7H_6NO)$ were observed. As the VUV wavelength changed from 118 to 157 nm, only $m/e=120(C_7H_6NO)$, $107(C_6H_4CH_3O)$, and $92(C_6H_4O)$ were observed. The image is shown in Fig. 9. The intensity profiles of $m/e=92$ and 120 obtained at 157 nm are the same as that of $m/e=120$ obtained at 118 nm. These three fragments must represent the fragment C_7H_6NO, corresponding to OH elimination. Photolysis laser intensities in the region of 0.4–30 mJ/cm^2 were used to determine the photon number dependence of these fragments. The results show that all above photofragments result from the dissociation of one-photon absorption.

The translational energy distributions of NO_2, NO, and OH elimination channels are shown in Fig. 10. The monotonic decrease of the probability with the increasing translational energy was observed for both NO_2 and OH elimination channels. However, two components in the translational energy distribution were clearly observed in the NO elimination channel.

In addition to the fragments described above, ions due to the fragment cracking upon ionization were also observed. They include the ions of $m/e=65$ from the cracking of fragment $C_6H_4CH_3$ and ions of $m/e=77$, 78, and 79 from the cracking of fragment $C_6H_4CH_3O$. However, the ion intensities are small.

Ion images from the photodissociation of 193 nm are similar to those of 248 nm, as illustrated in Fig. 11. Images

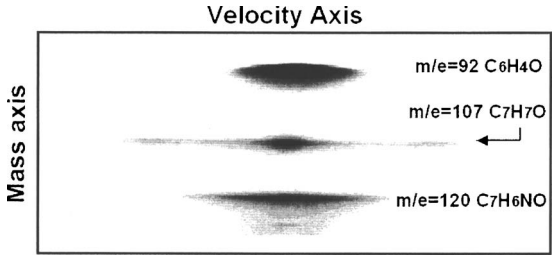

FIG. 9. Photofragment ion images from the photodissociation of *o*-nitrotoluene at 248 nm. The VUV wavelength is 157 nm.

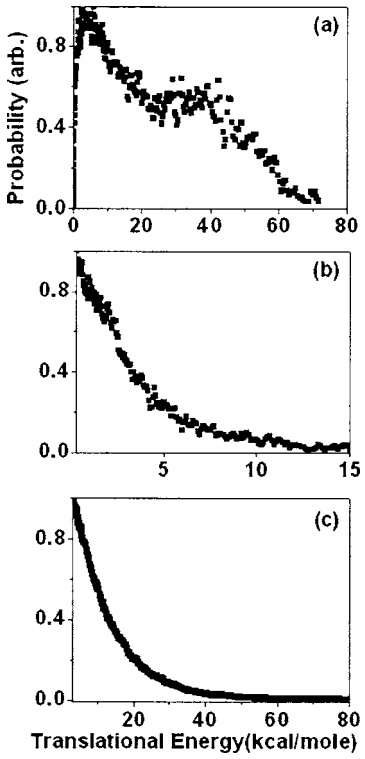

FIG. 10. Photofragment translational energy distribution of *o*-nitrotoluene at 248 nm. (a) $C_6H_4CH_3NO_2 \rightarrow C_6H_4CH_3O+NO$, (b) $C_6H_4CH_3NO_2 \rightarrow C_6H_4CH_3+NO_2$, and (c) $C_6H_4CH_3NO_2 \rightarrow C_7H_6NO+OH$.

of $m/e=46(NO_2)$ and $91(C_6H_4CH_3)$ have the largest intensities, corresponding to NO_2 elimination. Images of $m/e=30(NO)$ and $107(C_6H_4CH_3O)$ were also observed. Although the feature of two components in the translational energy distribution still remains in the NO elimination channel, as shown in Fig. 12, it is not as clear as that observed at 248 nm. The OH elimination channel is also observed from the fragments $m/e=119(C_7H_5NO)$ and $120(C_7H_6NO)$ at a VUV wavelength of 118 nm, as well as from the observation of fragment $m/e=120$ at a VUV wavelength of 157 nm, as illustrated in Fig. 11(f). Photolysis laser intensities in the region of 0.2–4 mJ/cm^2 were used to determine the photon

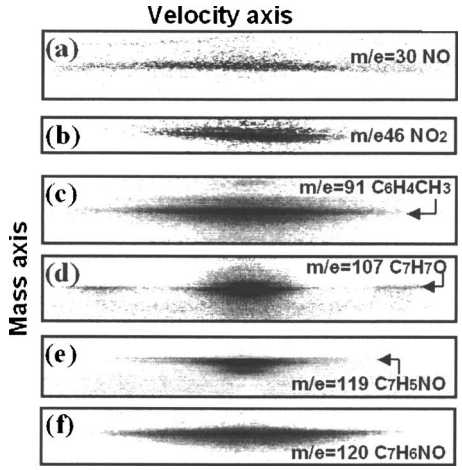

FIG. 11. Photofragment ion images from the photodissociation of *o*-nitrotoluene at 193 nm. The VUV wavelength is 118 nm for (a)–(e) and 157 nm for (f).

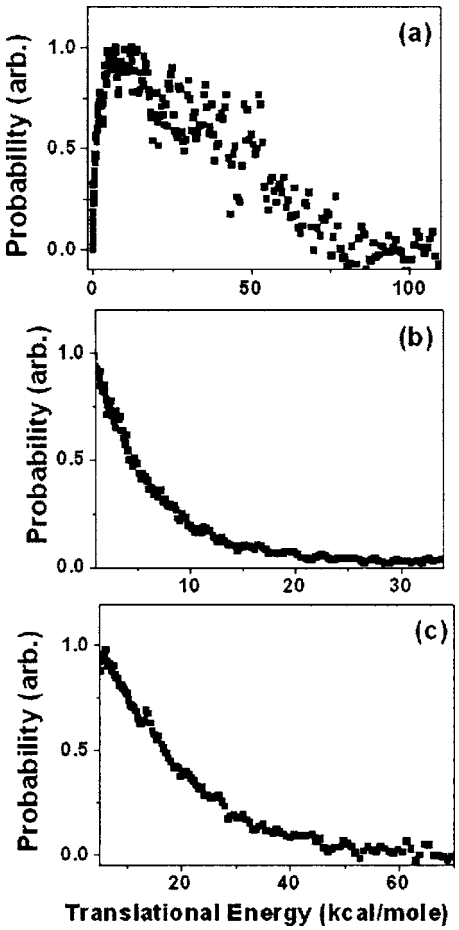

FIG. 12. Photofragment translational energy distribution of *o*-nitrotoluene at 193 nm. (a) $C_6H_4CH_3NO_2 \rightarrow C_6H_4CH_3O+NO$, (b) $C_6H_4CH_3NO_2 \rightarrow C_6H_4CH_3+NO_2$, and (c) $C_6H_4CH_3NO_2 \rightarrow C_7H_6NO+OH$.

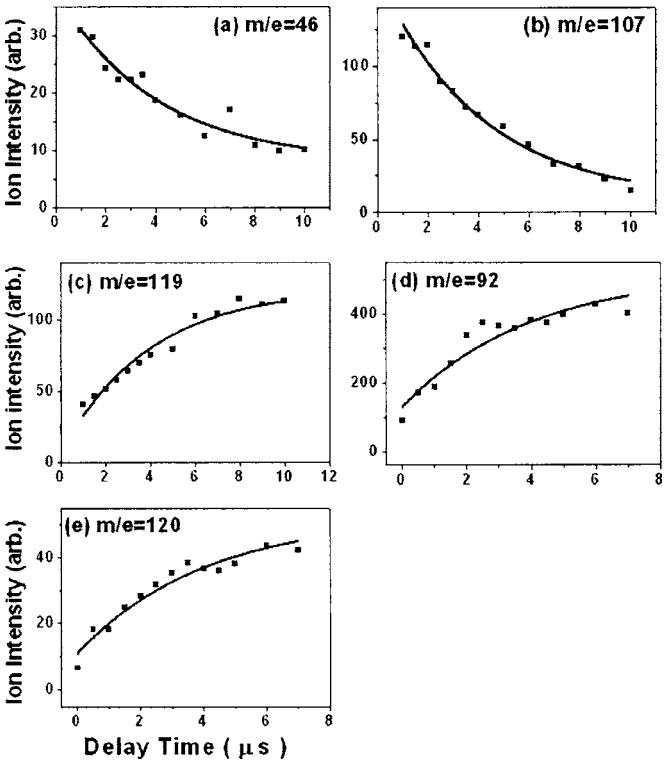

FIG. 13. Fragment ion intensity changes with respect to the delay time between pump and probe laser pulses. The photolysis wavelength is 248 nm; the VUV laser is 118.2 nm for (a)–(c) and 157 nm for (d) and (e). Solid squares are the experimental data. Solid lines are the fit to $A\exp(-kt)+B(1-\exp(-kt))$.

number dependence of these fragments. The results show that all of the above photofragments resulted from the dissociation of one-photon absorption.

The product growths with respect to the delay time between pump and probe laser pulses at 193 nm were found to be close to our instrument time response. The actual dissociation rate must be too fast to be measured ($>7\times10^7$ s^{-1}). A dissociation rate of 2.5×10^5 s^{-1} was obtained at 248 nm. The experimental data are shown in Fig. 13. No significant evidence of two dissociation rates can be found from the NO elimination channel product $m/e=107(C_6H_4CH_3O)$.

C. Dissociation branching ratios

The relative branching ratios of two major dissociation channels, NO elimination and NO_2 elimination, can be determined from the ion intensities after the normalization by the ionization cross sections at the corresponding VUV wavelength and the correction of the fragment velocity effect. The ionization cross sections of NO, NO_2, and C_6H_5 at 118 nm are 2.3, 0.23, and 17 Mb, respectively.[19(a)–19(c)] The relative ionization cross sections of NO_2 and C_6H_5 can be further checked by the following argument. In the photodissociation of nitrobenzene, one of the major channels is $C_6H_5NO_2 \rightarrow C_6H_5+NO_2$. The relative ion intensity of $C_6H_5^+$ and NO_2^+ measured by the same VUV wavelength (118.2 nm) after the correction of the fragment velocity effect is 79:1. Since these two fragments resulted from the same dissociation channel of nitrobenzene and the VUV photon energy is much higher than the ionization potential of these two fragments, the relative ion intensity measured in this experiment gives a good estimation of the relative ionization cross sections of these two fragments at this VUV laser wavelength. This ratio is consistent with the relative ionization cross sections from the literature. The similar calculation was used to confirm the relative ionization cross sections between NO and C_6H_5. The ion intensity ratio between NO and C_6H_5 obtained from the photodissociation of C_6H_5NO is 0.16,[19(d)] which is also very close to the relative ionization cross sections from the literature. As a result, the branching ratios between NO and NO_2 elimination channels of nitrobenzene were determined to be 0.32 ± 0.12, 0.26 ± 0.12, and 0.4 ± 0.12 for 193, 248, and 266 nm, respectively. A similar calculation was performed to obtain the relative branching ratio of NO elimination and NO_2 elimination for *o*-nitrotoluene. The values are 0.42 ± 0.12 and 0.3 ± 0.12 at 193 and 248 nm, respectively.

D. The calculations of the excited singlet and triplet states of nitrobenzene

The geometry of $C_6H_5NO_2$ (S_0) is a planar structure with a C_{2v} symmetry.[9] The geometry of $C_6H_5NO_2$ (T_1) is a nonplanar structure with a C_s symmetry. The ONCC dihedral angle calculated at the B3LYP/6-311G(d,p) level is 16.0°. The relative energy of T_1 to S_0 predicted with the G2M

TABLE I. Relative energy of T_1 at the G2M(RCC,MP2)//B3LYP/6-311(d,p) level, vertical excitation energies of S_1-S_8 and T_2-T_8 excited states in kcal mol^{-1} and oscillator strengths (f) of nitrobenzene (NB) and *o*-nitrotoluene (*o*-NT) estimated by TD-DFT at the B3LYP/6-311(d,p) level.

	Singlet states					Triplet states				
Molecule	State	Symmetry	Excitation E	Oscillator strengths	Expt.	State	Symmetry	Excitation E	Oscillator strengths	Expt.
NB	S_1	$^1A_2$	88.6	0.0000	81.7[a]	T_1	$^3A'$	72.8		62.9–77.2[b]
	S_2	$^1B_1$	99.8	0.0001	102.1[c]	T_2	$^3A'$	84.1	0.0003	
	S_3	$^1B_2$	103.0	0.0139	102.1[c]	T_3	$^3A''$	109.3	0.0012	
	S_4	$^1A_1$	112.4	0.1928	115.3[d]	T_4	$^3A''$	116.7	0.0071	
	S_5	$^1B_2$	138.7	0.0001		T_5	$^3A'$	117.4	0.0001	
	S_6	$^1B_2$	141.2	0.0550		T_6	$^3A'$	151.4	0.0043	
	S_7	$^1B_1$	145.1	0.0000	148.1[e]	T_7	$^3A''$	154.5	0.0002	
	S_8	$^1A_2$	152.5	0.0000	148.1[e]	T_8	$^3A'$	165.2	0.0015	
o-NT	S_1	^1A	88.0	0.0075		T_1	^3A	71.1		76.2[f]
	S_2	^1A	98.5	0.0196		T_2	^3A	84.5	0.0003	
	S_3	^1A	100.6	0.0104		T_3	^3A	108.3	0.0018	
	S_4	^1A	112.5	0.1460	115.3[g]	T_4	^3A	113.5	0.0020	
	S_5	^1A	134.7	0.0065	126.5[h]	T_5	^3A	115.8	0.0065	
	S_6	^1A	141.2	0.0306		T_6	^3A	148.6	0.0030	
	S_7	^1A	145.3	0.0940	148.1[c]	T_7	^3A	152.3	0.0011	
	S_8	^1A	147.3	0.0130	148.1[c]	T_8	^3A	161.9	0.0014	

[a]The band observed by Tsai *et al.* [Ref. 20(a)].
[b]The band observed by Takezaki *et al.* [Ref. 20(b)].
[c]The band observed by Nagakura *et al.* (Ref. 21).
[d]The band observed by Marshall *et al.* (Ref. 23) and this work.
[e]The band observed by this work.
[f]The band observed by Kosmidis *et al.* (Ref. 5).
[g]The band observed by Marshall *et al.* (Ref. 24) and this work.
[h]The band observed by Marshall *et al.* (Ref. 2) and Castle *et al.* (Ref. 7).

(RCC, MP2) method is 72.8 kcal/mol. Takezaki *et al.* calculated the geometries and energies of $C_6H_5NO_2$ in the ground and excited states using the CASSCF method.[8] In their work, the relative energy of T_1 to S_0 was 52.5 kcal/mol using CASSCF with the dzv N^* basis and 58.0 kcal/mol with the dzp basis. Our predicted value (72.8 kcal mol^{-1}) is in good agreement with the experimental energy of 62.9–77.2 kcal/mol measured also by Takezaki *et al.*[20(b)]

The vertical excitation energies of the electronic excited states could be predicted reasonably by the TD-DFT method based on the ground state geometries.[13] The calculated vertical excitation energies of the electronic excited S_1-S_8 and T_2-T_8 states of $C_6H_5NO_2$ using TD-DFT at the B3LYP/6-311(d,p) level based on the optimized geometries of S_0 and T_1 at the same level, respectively, are summarized in Table I. According to these calculated values listed in Table I, some experimental absorption bands in the photodissociation of nitrobenzene can be assigned reasonably. A much weaker absorption band centered at 350 nm (81.7 kcal/mol) observed in previous reports[20(a)] may be assigned to S_1 with a negligibly small oscillator strength. This band was also assigned to S_1 in those studies.[20(a)] The second absorption band at 280 nm (102.1 kcal/mol) observed by Nagakura *et al.*[21] and Abbott *et al.*[22] may be assigned to a mixture of S_2 with an oscillator strength of 0.0001 and S_3 with an oscillator strength of 0.0139. The band at 280 nm assigned to S_1 by Nagagkura *et al.*[21] and Abbott *et al.*[22] might be incorrect. The third absorption band at 248 nm (115.3 kcal/mol) was observed by Marshall *et al.*[23] This absorption may be assigned to S_4 with the strongest oscillator strength of 0.1928. Finally, the absorption band at 193 nm (148.1 kcal/mol) observed in this work may be assigned to a mixture of S_7 and S_8 with a small oscillator strength.

E. The calculations of the excited singlet and triplet states of *o*-nitrotoluene

The relative energy of T_1 to S_0 with the G2M (RCC, MP2) method is 71.1 kcal/mol, which is somewhat lower than the experimental energy of T_1 of *o*-nitrotoluene [76.2 kcal/mol (Ref. 8)]. We also calculated the vertical excitation energies of the excited S_1-S_8 and T_2-T_8 states of *o*-nitrotoluene using TD-DFT at the B3LYP/6-311(d,p) level based on the optimized geometries of S_0 and T_1 at the same level, respectively. These excitation energies are also listed in Table I. According to Table I, some experimental absorption bands accessed in the photodissociation of *o*-nitrotoluene may also be more reasonably assigned. The absorption band at 375 nm (76.2 kcal/mol) in the photodissociation of *o*-nitrotoluene observed by the femtosecond mass spectroscopic technique[5] may be assigned to T_1. The second absorption band at 248 nm (115 kcal/mol) observed by Marshall *et al.*[24] and in this work may be assigned to S_4 with the strongest oscillator strength of 0.1460. The third absorption band at 226 nm (126.5 kcal/mol) observed by Marshall *et al.*[2] and Castle *et al.*[7] may be assigned to S_5 with an oscillator strength of 0.0065. Finally, the absorption band

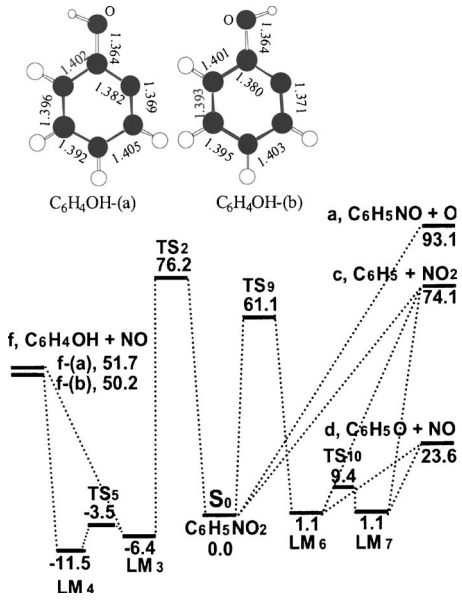

FIG. 14. Simplified potential energy surface for various dissociation channels, where energy units are in kcal/mol. For the details of structures, please see Ref. 9.

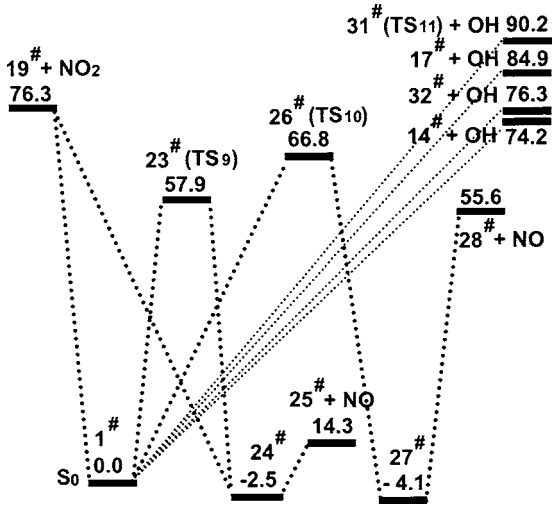

FIG. 15. Simplified potential energy surface for various dissociation channels, where energy units are in kcal/mol. For the details of structures, please see Ref. 10.

at 193 nm (148.1 kcal/mol) observed in this work may be assigned to a mixture of S_7 with an oscillator strength of 0.0094 and S_8 with an oscillator strength of 0.0130.

F. Prediction for dissociation rates and lifetimes of photodissociation of nitrotoluene and *o*-nitrotoluene

Assuming that the internal conversion is fast compared with fragmentation lifetimes, we can predict the fragmentation rates of nitrobenzene and *o*-nitrotoluene following the UV excitation on the basis of the RRKM theory using the VARIFLEX code[16] and the CHEMRATE program.[17] The dissociation rate $k(E_l)$ corresponds to the microcanonical unimolecular dissociation rate at the internal energy E_i of 107.7 kcal/mol for 266 nm, 115.3 kcal/mol for 248 nm, and 148.1 kcal/mol for 193 nm, and the fragmentation lifetime is $1/k(E_i)$.

The primary photodissociation channels of nitrobenzene at 266, 248, and 193 nm are NO_2 elimination, NO elimination, and a small amount of O atom elimination. There are two channels for NO elimination producing C_6H_5O and C_6H_4OH. Most of the potential energy surface for the decomposition of nitrobenzene has been published previously.[9] The simplified potential energy surface is illustrated in Fig. 14. As shown in the figure, the two decomposition channels for NO fragmentation as alluded to above take place by the following low energy paths:

$$C_6H_5NO_2 \xrightarrow{TS_9} LM_6, LM_7 \rightarrow C_6H_5O + NO,$$

$$C_6H_5NO_2 \xrightarrow{TS_2} LM_3, LM_4 \rightarrow C_6H_4OH + NO,$$

where TS_9 with a barrier of 61.1 kcal/mol and TS_2 with a barrier of 76.2 kcal/mol control primarily their corresponding decomposition processes. The structures of these TS's and the identifications of various intermediates denoted by the local minima (LM_n) were published in a previous study.[9] For the photodissociation of *o*-nitrotoluene at 248 and 193 nm, the primary observed fragments are NO_2, NO, and OH. The potential energy surface for the decomposition of *o*-nitrotoluene has been reported.[10] The simplified potential surface is shown in Fig. 15. As shown in Fig. 15, there are two channels for NO elimination and many product isomers for OH fragmentations given as follows:

$$1^{\#} \xrightarrow{TS_9} 24^{\#} \rightarrow 25^{\#} + NO,$$

$$1^{\#} \xrightarrow{TS_{10}} 27^{\#} \rightarrow 28^{\#} + NO,$$

$$1^{\#} \rightarrow 14^{\#}, 17^{\#}, 31^{\#}, 32^{\#} + OH,$$

where the species $1^{\#}$ represents *o*-nitrotoluene (*o*-NT). TS_9 with a barrier of 57.9 kcal/mol for the formation of $CH_3C_6H_5O(25^{\#})+NO$ and TS_{10} with a barrier of 66.8 kcal/mol for the formation of $CH_2(OH)C_6H_4(28^{\#})+NO$ control primarily their corresponding decomposition channels. The channel for the formation of $C_6H_4C(H_2)NO(14^{\#})+OH$ with a lower endothermicity of 74.2 kcal/mol is the primary decomposition channel for OH fragmentation. This process takes place variationally in its final stage of fragmentation.

The calculation for the dissociation rates and lifetimes of nitrobenzene (NB) and *o*-NT producing $C_6H_5+NO_2$ and $CH_3C_6H_5+NO_2$, as described for the thermal decomposition of both compunds,[9,10] has been made with the VARIFLEX code[16] based on the minimum energy paths derived for both processes. The calculation for the dissociation rates producing C_6H_5O+NO and C_6H_4OH+NO for NB and $CH_3C_6H_5O(25^{\#})+NO$, $CH_2(OH)C_6H_4(28^{\#})+NO$, and $C_6H_4C(H_2)NO(14^{\#})+OH$ for *o*-NT involving multiple wells was carried out with the CHEMRATE program.[17]

The predicted dissociation rates and lifetimes for the primary pathways of each molecule are listed in Table II. The lifetimes for the C_6H_5O+NO from NB are 10–20 times

TABLE II. Calculated dissociation rates $k(E)$ and lifetimes of photodissociation of nitrobenzene (NB), triplet nitrobenzene (T-NB), and *o*-nitrotoluene (*o*-NT) via different pathways.

		Dissociation rate (s^{-1})			Lifetime (ps)		
Molecule	Pathway	266 nm	248 nm	193 nm	266 nm	248 nm	193 nm
NB	NB+$h\nu\rightarrow$ $C_6H_5+NO_2(^2A_1)$	8.0×10^7	3.0×10^8	2.1×10^{10}	1.3×10^4	3.3×10^3	4.8×10^1
	NB+$h\nu\rightarrow$ C_6H_5O+NO	7.2×10^6	2.7×10^7	1.2×10^9	1.4×10^5	3.7×10^4	9.0×10^2
	NB+$h\nu\rightarrow$ C_6H_4OH+NO	7.8×10^2	6.0×10^3	2.0×10^6	1.3×10^9	1.7×10^8	5.0×10^5
T-NB	T-NB+$h\nu\rightarrow$ $C_6H_5+NO_2(^2B_2)$	8.6×10^5	3.8×10^7	1.9×10^{10}	1.2×10^6	2.7×10^4	5.4×10^1
	T-NB+$h\nu\rightarrow$ C_6H_5O+NO	1.9×10^8	8.4×10^8	1.9×10^{10}	5.4×10^3	1.2×10^3	5.3×10^1
o-NT	*o*-NT+$h\nu\rightarrow$ $CH_3C_6H_4+NO_2$	3.4×10^6	2.3×10^7	3.4×10^9	2.9×10^5	4.4×10^4	2.9×10^2
	o-NT+$h\nu\rightarrow$ $CH_3C_6H_4O+NO$	1.3×10^6	4.5×10^6	2.0×10^8	7.8×10^5	2.2×10^5	5.0×10^3
	o-NT+$h\nu\rightarrow$ $CH_2OHC_6H_4+NO$	5.7×10^3	3.2×10^4	4.3×10^6	1.8×10^8	3.1×10^7	2.3×10^5
	o-NT+$h\nu\rightarrow$ $CH_2C_6H_4NO+OH$	9.2×10^5	2.3×10^6	3.7×10^7	1.1×10^6	4.4×10^5	2.7×10^4

longer than those for the NO_2 formation pathway. The lifetimes for the second NO fragmentation pathway of NB producing C_6H_4OH are 5–100 hundred times longer than those for the C_6H_5O formation path.

In comparison, the lifetimes for *o*-NT fragmentation producing $CH_3C_6H_4+NO_2$ (from $CH_3C_6H_4NO_2$ directly, not from $24^{\#}$) are about 6–13 times longer than those for the $C_6H_5+NO_2$ production from NB. The lifetimes for *o*-NT fragmentation producing $CH_3C_6H_5O+NO$ are about five times longer than those for the C_6H_5O+NO production from NB at the same wavelengths. The lifetimes for *o*-NT dissociation by the second NO fragmentation path producing $CH_2OHC_6H_4+NO$ at 248 and 193 nm are 46–140 times longer than those for the first NO fragmentation process at the same wavelengths. The total dissociation rates of NB at 266, 248, and 193 nm are 8.7×10^7, 3.3×10^8, 2.2×10^{10} s^{-1}, and those of *o*-NB at 248 and 193 nm are 3×10^7 and 3.6×10^9 s^{-1}, respectively. The dissociation rate for nitrobenzene at 266 nm is close to the experimental value.

V. DISCUSSION

As discussed in the preceding section, the decomposition of $C_6H_5NO_2$ into C_6H_5 and NO_2 can occur directly or after the isomerization to C_6H_5ONO. As shown in Fig. 14, the dissociation from both nitrobenzene and phenyl nitrite are direct dissociation processes. However, once the NB isomerizes to C_6H_5ONO, the decomposition into C_6H_5O+NO is more likely to occur due to the lower dissociation energy. Therefore, unlike the decomposition mechanism suggested in a previous study,[3] the direct fragmentation from NB plays a major role in the NO_2 elimination channel. Similarly, as shown in Fig. 15, the decomposition of *o*-NT into *o*-$CH_3C_6H_4$ and NO_2 should occur directly, with a negligible contribution from $CH_3C_6H_4ONO(24^{\#})$ after isomerization.

The bimodal translational energy distribution in the NO elimination channel of NB indicates a much more complicated dissociation mechanism than that proposed in a previous study.[4] The energy difference between the peaks of slow and fast components from the photodissociation of NB at 193 nm is about 22 kcal/mol. In comparison, the energy difference between the fast and slow components from the photodissociation of *o*-NT is more than 30 kcal/mol. One of the possible mechanisms is that there are two NO elimination channels for both NB and *o*-NT in the ground electronic state, as alluded to above. For the two NO elimination channels of NB shown in Fig. 14, the transition state TS_2 with a barrier of 76.2 kcal/mol primarily controls the second NO elimination channel of C_6H_4OH+NO, whose energy is 15 kcal/mol higher than the barrier of the primary NO elimination channel of C_6H_5O+NO. In addition to the difference in barrier heights, the difference in the heats of reaction is as large as 26 kcal/mol. The large difference in the heats of reaction between these two channels might result in the large difference in the release of translational energy, as illustrated in Fig. 2. The slow component corresponds to C_6H_4OH+NO, which has a larger heat of reaction, and the fast component corresponds to C_6H_5O+NO, which has a smaller heat of reaction. A similar dissociation mechanism can be applied to *o*-NT. As shown in Fig. 15, the transition state TS_{10} with a barrier of 66.8 kcal/mol primarily controls the second NO elimination channel of $CH_2(OH)C_6H_4(28^{\#})+NO$, whose energy is 9 kcal/mol higher than the barrier of the primary NO elimination channel of $CH_3C_6H_5O(25^{\#})+NO$. The difference in the heats of reaction between these two channels is 41 kcal/mol, which is larger than the corresponding value of NB (26 kcal/mol). This possible mechanism explains the

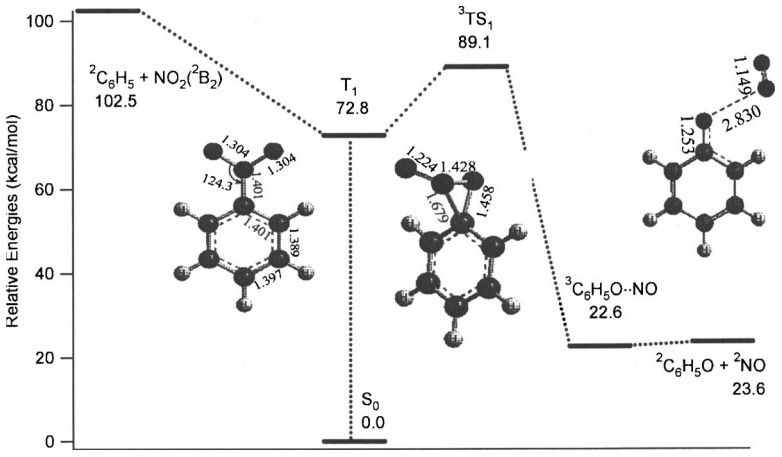

FIG. 16. Schematic energy diagram of nitrobenzene for the primary dissociation reactions of T_1 at the G2M(RCC,MP2)‖B3LYP/6-311G(d,p) level, where energy units are in kcal/mol.

NO bimodal distribution in translational energy. However, it cannot explain the wavelength dependence of the ratio between fast and slow components. This is because the slow component (C_6H_4OH+NO) has a larger barrier height and it should decrease more rapidly as the photolysis wavelength increases. It is not consistent with the experimental results.

Another possible mechanism for the nitrobenzene NO elimination channel is that more than one electronic state are involved in the dissociation processes. For example, the dissociation from the triplet state can also lead to the same product, as shown in Fig. 16. In the triplet state, dissociation after passing the transition state only goes by an intermediate with a very shallow potential well (1 kcal/mol below the products) and leads directly into the products. As a result, the energy release into the translational energy could be large. On the other hand, dissociation from the ground state after passing the transition state has to pass two intermediates (LM_6 and LM_7). The potential wells of these two intermediates are about 23 kcal/mol below the products. The translational energy release in this channel may be small. Since the barrier height from the triplet state is larger than that from the ground state, it explains the photolysis wavelength dependence of the ratio between fast and slow components in the NO elimination channel.

In addition, if the other electronic excited states are involved in the dissociation process, phenoxy radicals may be produced in two electronic states. The energy difference between the ground electronic state and the first electronic excited state of phenoxy radical is about 24.5 kcal/mol,[25] which is similar to the energy difference between the fast and slow components. A similar argument can be applied to *o*-nitrotoluene. However, due to the lack of the excited state potential energy surface, we cannot determine these possible mechanisms solely from experimental data.

For *o*-NT, an additional channel such as OH elimination was observed. This channel was also reported in previous studies.[5,6,26] The possible dissociation mechanism is shown in Fig. 15. The potential energy diagram shows that there are two dissociation pathways of *o*-NT$\rightarrow CH_2C_6H_4N(O)OH \rightarrow C_6H_4C(H_2)NO(14^{\#})+OH$ and *o*-NT$\rightarrow CH_2C_6H_4$-*t*-N(OH)O or $CH_2C_6H_4$-*c*-N(OH)O$\rightarrow CH_2C_6H_4NO(17^{\#})+OH$ with 74.2 and 84.9 kcal/mol overall endothermicities, respectively. The first pathway is the primary channel for OH elimination, which was observed in the photodissociation experiment.

ACKNOWLEDGMENTS

The work was supported by the National Science Council, Taiwan under Contract No. NSC 94-2113-M-001-036. Two of the authors (M.C.L.) and (S.C.X.) are grateful to the support of this work from the Basic Energy Sciences, Department of Energy under Contract No. DE-FG02-97-ER14784 M.C.L. also acknowledges the support from the National Science Council of Taiwan for a Distinguished Visiting Professorship at National Chiao Tung University in Hsichu, Taiwan.

[1] V. H. Schuler and A. Woeldike, Phys. Z. **45**, 171 (1944); S. H. Hastings and F. A. Matsen, J. Am. Chem. Soc. **70**, 3514 (1948); G. Porter and B. Ward, Proc. R. Soc. London, Ser. A **303**, 139 (1968).
[2] A. Marshall, A. Clark, K. W. D. Ledingham, J. Sander, and R. P. Singhal, Int. J. Mass Spectrom. Ion Process. **124**, R15 (1993).
[3] D. B. Galloway, J. A. Bartz, L. G. Huey, and F. F. Crim, J. Chem. Phys. **98**, 2107 (1993).
[4] D. B. Galloway, T. Glenewinkel-Meyer, J. A. Bartz, L. G. Huey, and F. F. Crim, J. Chem. Phys. **100**, 1946 (1994); Y.-M. Li, J.-L. Sun, H.-M. Yin, K.-L. Han, and G.-Z. He, *ibid.* **118**, 6244 (2003).
[5] C. Kosmidis, K. W. D. Ledingham, H. S. Kilic, T. McCanny, R. P. Singhal, A. J. Langley, and W. Shaikh, J. Phys. Chem. A **101**, 2264 (1997).
[6] J. Shao and T. Baer, Int. J. Mass Spectrom. Ion Process. **86**, 357 (1988).
[7] K. J. Castle, J. E. Abbott, X. Peng, and W. Kong, J. Phys. Chem. A **104**, 10419 (2000).
[8] M. Takezaki, N. Hirota, M. Terazima, H. Sato, T. Nakajima, and S. Kato, J. Phys. Chem. A **101**, 5190 (1997).
[9] S. C. Xu and M. C. Lin, J. Phys. Chem. B **109**, 8367 (2005).
[10] S. C. Chen, S. C. Xu, E. Diau, and M. C. Lin, J. Phys. Chem. A **110**, 10130 (2006).
[11] S. T. Tsai, Y. T. Lee, and C. K. Ni, J. Phys. Chem. A **104**, 10125 (2000); S. T. Tsai, C. K. Lin, Y. T. Lee, and C. K. Ni, J. Chem. Phys. **113**, 67 (2000); Rev. Sci. Instrum. **72**, 1963 (2001); S. T. Tsai, C. L. Huang, Y. T. Lee, and C. K. Ni, J. Chem. Phys. **115**, 2449 (2001).
[12] A. M. Mebel, K. Morokuma, and M. C. Lin, J. Chem. Phys. **103**, 7414 (1995).
[13] R. E. Stratmann, G. E. Scuseria, and M. J. Frisch, J. Chem. Phys. **109**, 8218 (1998); M. E. Casida, C. Jamorski, K. C. Casida, and D. R. Salahub, *ibid.* **108**, 4439 (1998).
[14] M. J. Frisch, G. W. Trucks, H. B. Schlegel *et al.*, GAUSSIAN 98, Revision A.7, Gaussian, Inc., Pittsburgh, PA, 2003.
[15] R. D. Amos, A. Bernhardsson, A. Berning *et al.*, MOLPRO, Version 98.1, University of Birmingham, Birmingham, UK, 1998.
[16] S. J. Klippenstein, A. F. Wagner, R. C. Dunbar, D. M. Wardlaw, and S. H. Robertson, VARIFLEX, 1999.

[17] W. Mokrushin, V. Bedanov, W. Tsang, M. Zachariah, and V. Knyazev, CHEMRATE, Version 1.20, National Institute of Standards and Technology Gaithersburg, MD 20899, 2003.
[18] C.-Y. Lin and M. C. Lin, J. Phys. Chem. **90**, 425 (1986).
[19] (a) T. Nakayama, M. Y. Kitamura, and K. Watanabe, J. Chem. Phys. **30**, 1180 (1959); (b) K. Watanabe, *ibid.* **22**, 1564 (1954); (c) N. E. Sveum, S. J. Goncher, and D. M. Neumark, Phys. Chem. Chem. Phys. **8**, 592 (2006); (d) C. M. Tzeng, Y. M. Choi, C. L. Huang, C. K. Ni, Y. T. Lee, and M. C. Lin, J. Phys. Chem. A **108**, 7928 (2004).
[20] (a) B. Vidal and J. N. Murrell, Chem. Phys. Lett. **31**, 46 (1975); (b) M. Takezaki, N. Hirota, and M. Terazima, J. Phys. Chem. A **101**, 3443 (1997).
[21] S. Nagagkura, M. Kojima, and Y. Maruyama, J. Mol. Spectrosc. **13**, 174 (1964).
[22] J. E. Abbott, X. Peng, and W. Kong, J. Chem. Phys. **117**, 8670 (2002).
[23] A. Marshall, A. Clark, R. Jennings, K. W. D. Ledingham, and R. P. Singhal, Int. J. Mass Spectrom. Ion Process. **112**, 273 (1992).
[24] A. Marshall, A. Clark, R. Jennings, K. W. D. Ledingham, J. Sander, and R. P. Singhal, Int. J. Mass Spectrom. Ion Process. **116**, 143 (1992).
[25] J. G. Radziszewski, M. Gil, A. Gorski, J. Spanget-Larsen, J. Waluk, and B. J. Mroz, J. Chem. Phys. **115**, 9733 (2001).
[26] S. A. McLuckey and G. L. Glish, Org. Mass Spectrom. **22**, 224 (1987).